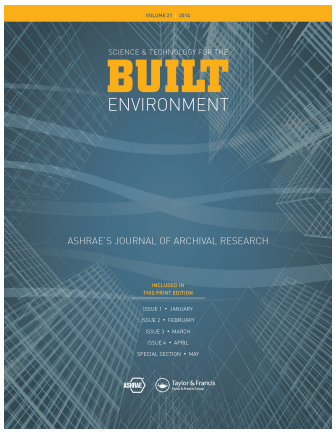

Science and Technology for the Built Environment
Publication details, including instructions for authors and subscription information:
http://www.tandfonline.com/loi/uhvc21

Fault-tolerant optimal control of a building heating, ventilation, and air conditioning system

Sorin C. Bengea[a], Pengfei Li[b], Soumik Sarkar[c], Sergey Vichik[d], Veronica Adetola[a], Keunmo Kang[a], Teems Lovett[e], Francesco Leonardi[e] & Anthony D. Kelman[d]

[a] Control Systems group at the United Technologies Research Center, 411 Silver Lane, MS-129-85, East Hartford, CT 06108

[b] Thermo-Fluid Dynamics group at the United Technologies Research Center, East Hartford, CT

[c] Mechanical Engineering Department at Iowa State University

[d] Department of Mechanical Engineering, University of California, Berkeley, CA

[e] Embedded Systems group at the United Technologies Research Center, East Hartford, CT

Accepted author version posted online: 06 Jul 2015.

To cite this article: Sorin C. Bengea, Pengfei Li, Soumik Sarkar, Sergey Vichik, Veronica Adetola, Keunmo Kang, Teems Lovett, Francesco Leonardi & Anthony D. Kelman (2015): Fault-tolerant optimal control of a building heating, ventilation, and air conditioning system, Science and Technology for the Built Environment, DOI: 10.1080/23744731.2015.1057085

To link to this article: http://dx.doi.org/10.1080/23744731.2015.1057085

Fault-tolerant optimal control of a building heating, ventilation, and air conditioning system

Sorin C. Bengea[1*], Pengfei Li[2], Soumik Sarkar[3], Sergey Vichik[4], Veronica Adetola[1], Keunmo Kang[1], Teems Lovett[5], Francesco Leonardi[5], and Anthony D. Kelman[4]

[1]Control Systems group at the United Technologies Research Center, 411 Silver Lane, MS-129-85, East Hartford, CT 06108.

[2]Thermo-Fluid Dynamics group at the United Technologies Research Center , East Hartford, CT.

[3]Mechanical Engineering Department at Iowa State University.

[4]Department of Mechanical Engineering, University of California, Berkeley, CA.

[5]Embedded Systems group at the United Technologies Research Center, East Hartford, CT.

Received December 9, 2014; accepted March 19, 2015.

Corresponding author e-mail: bengeasc@utrc.utc.com

Sorin C. Bengea, PhD, is a Principal Research Engineer. **Pengfei Li, PhD,** is a Senior Research Engineer. **Soumik Sarkar, PhD,** is an Assistant Professor. **Sergey Vichik** is a doctoral student. **Veronica Adetola, PhD,** is a Staff Research Engineer. **Keunmo Kang, PhD,** is a Staff Research Engineer. **Teems Lovett, PhD,** is a Principal Research Engineer. **Francesco Leonardi, PhD,** is a Senior Research Engineer. **Anthony D. Kelman** is a doctoral student.

The paper[1] *presents the development and application of a fault-tolerant control (FTC) technology, its on-line implementation, and results from several tests conducted for a large-sized HVAC system. By integrating model-based Model Predictive Control (MPC) and data-driven Fault Detection and Diagnostics (FDD) algorithms, the technology automatically adapts the HVAC control laws to a set of subsystem faults, and therefore can reach and maintain the largest energy consumption reduction levels that are achievable at any point throughout a building lifecycle. The MPC algorithm generates optimal set points, which minimize energy consumption, for the HVAC actuator loops while meeting equipment operational constraints and occupant thermal-comfort constraints. The FDD algorithm uses probabilistic graphical models to detect and classify in real-time potential faults of the HVAC actuators based on data from multiple sensors. The FTC system is realized by executing the two algorithms on the same platform, within the same framework, and by using the FDD algorithm's output to continuously update the MPC algorithm constraints. The proposed integrated technology is executed at the supervisory level in a hierarchical control architecture, as an extension of a baseline Building Management System (BMS). The performance and limitations of the FDD, MPC and FTC algorithms are illustrated and discussed using measurement data recorded from multiple tests.*

Keywords: Building Automation & Controls, Commercial Buildings, Controls, Research & Development

[1] This is an extension of the paper (Bengea *et al.*, 2014) presented at 3rd International High Performance Buildings Conference at Purdue, July 14-17, 2014, West Lafayette, IN.

INTRODUCTION

The large potential economic impact of advanced technologies underlying modern Building Management Systems (BMS) have led to increased efforts focused on developing, designing, and implementing model-based control and diagnostics technologies for building HVAC systems with the objective to estimate their cost effectiveness. The potential economic impact is apparent both from the high energy-consumption levels of building HVAC systems, estimated currently at 27% (EPA, 2008), and from limitations of existing control technologies for HVAC systems. Model-based paradigms have been employed to integrate in a direct and systematic way sensor data from multiple subsystems with the objective to generate optimal set-points that lead to an increased overall efficiency. Implementation of model-based algorithmsð requiring more communication and computational resources than traditional control systemsð has been facilitated by the availability of modern BMS platforms and open communication infrastructures.

This paper presents an optimal, fault-tolerant control technology that integrates equipment fault diagnostics and optimal set-point control algorithms at supervisory level, as an extension of a baseline Building Management System (BMS). The focus is on their development, implementation, and performance estimation based on the results of tests conducted in two commercial buildings. Integration of the two technologies into the same model-based framework addresses two major challenges in building control systems: cost of deployment, and optimization of the HVAC system efficiency throughout its life. Although previous efforts (Adetola *et al.*, 2013; Bengea *et al.*, 2014) have demonstrated energy savings separately for diagnostics and optimal control algorithms at various building scales, the model-based technologies have not always led to cost-effective solutions due to the cost of commissioning of

instrumentation and algorithms. The effort described herein minimizes these costs in two ways. First, by deploying the MPC and FDD algorithms on the same platform, within the same framework, using the same sensor suites for model development and real-time execution. Second, by employing an automated tool for formulating optimization problems associated with MPC algorithms for large-size HVAC systems.

The integrated framework proposed here has the potential to maximize the building system efficiency throughout its lifetime by implementing the fault-tolerant algorithm in which the diagnostics algorithmôs output is used to periodically update the MPC algorithm constraints. For a healthy system, when no faults are present, the MPC algorithm generates solutions that are practically optimal. When faults are detected, the algorithm generates solutions that are optimal within the new actuator constraintsð when comfort constraints can be met. When the magnitudes of the faults impede satisfaction of comfort constraints, the control algorithm minimizes the discomfort level to the extent possible within these constraints. The existing fault-tolerant control design methods can be categorized into two main groups: passive and active (Zhang and Jiang, 2008). The passive schemes are similar to robust control approaches in the sense that the controls are designed conservatively to accommodate selected potential faults. The active methods, on the other hand, are adaptive; they react to system failure in real time by reconstructing the control actions to eliminate or attenuate the impact of the identified faults. Active FTC requires fault diagnostic tools and can cope with a greater range of faults and variations in system behavior than passive FTC systems.

There has been a recent surge in the development and demonstration of FTC for building and HVAC applications in order to address the increased demands for energy savings, system

reliability and efficient operation. Application of active FTC in buildings domain includes (Fernandez *et. al*, 2009; Wang and Cheng, 2002) where an FTC algorithm was demonstrated in simulation for detecting and correcting sensor and damper faults in air handling units. For VAV air conditioning systems, (Liu and Dexter, 2001) applies a supervisory fuzzy logic based FTC to characterize and correct for fouling performance degradation faults and (Talikdar and Patra, 2010) presents an approach that accommodates stuck damper vanes of the air handler.

Fault detection and diagnostics technologies have significant potential to reduce energy inefficiencies resulting from faults and degradation of building equipment and materials; errors in operating schedules and critical design/planning flaws. A comprehensive literature review can be found in (Katipamula 2005a, and 2005b) where the FDD methods are broadly categorized into two classes, namely model-based and data-driven. Model-based techniques primarily involve either physics-based models, such as APAR rules in (Schein, 2006), sophisticated Modelica models in (Wetter 2009), EnergyPlus simulation models in (Pedrini *et al.*, 2002)) or empirical models, such as extended Kalman Filter in (Yoshida, 1996). Although model-based techniques perform well, often calibration and validation of such models may become expensive. Data-driven techniques have the advantage that they require a reduced calibration and validation effort; they range from simple statistical analysis (Seem 2007), principal component analysis (Xiao and Wang, 2009) to complex machine learning models, such as artificial neural network (Peitsman and Bakker, 1996). The algorithm implemented for this effort uses a probabilistic graphical-model based technique to model the historical performance of various HVAC subsystems in a data-driven manner. Specific faults of HVAC actuators, such as dampers and valves are flagged and diagnosed in real-time upon detection of any deviations from the modeled

nominal behavior. Based on experimental data, it was estimated that the FDD algorithm correctly diagnosed the HVAC subsystem faults in 84% of the cases, missed the detection of 6% of the events, and generated false alarms in 10% of the cases when faults were seeded.

Model Predictive Control technologies are applied optimal control algorithms that use dynamical and steady-state models and predictions of plant disturbances to minimize a selected performance cost while satisfying operation and equipment constraints (Morari and Lee 1999; Mayne et al. 2000; Borrelli 2003). In this effort, an MPC algorithm was implemented at supervisory level to periodically solve an optimization problem and generate optimal sequences of set points for Air Handling Units (AHUs) and Variable Air Volume units (VAVs). A similar hierarchical architecture has been proposed in (Kelly 1988). Simulation and experimental results have been reported previously for smaller scale HVAC systems (Henze *et al.* 2004, 2005, Clarke *et al.* 2002, Li *et al.* 2012 and 2014), and for radiant HVAC systems (Siroky *et al.* 2011). A similar implementation of an MPC technology, as the one described here, was reported in (Bengea *et al.* 2014) for a medium-scale Multi-Zone Unit for a commercial building. The efforts presented herein build on this previous implementation by employing the Berkeley Library for Optimization Modeling (BLOM) (Kelman, Vichik, and Borrelli, 2013) to automatically formulate the MPC algorithm and implementing it for a large-scale building. This new computational toolbox significantly reduces the development effort of translating nonlinear simulation-oriented models into efficient constrained optimization problem formulations for MPC. The performance results, estimated based on sensor measurements and meter data, indicate that MPC algorithm reduced energy consumption by more than 20% while improving thermal comfort.

The paper is organized as follows. Section ñBuilding HVAC System and Control-Oriented Modelsò describes the HVAC system configuration and the models used for MPC design. The FDD algorithm design and calibration is presented in the section ñFault Detection and Diagnostics Algorithmsò. Section ñFormulations and Implementations of Model Predictive and Fault-Tolerant Control Algorithmsò presents the MPC algorithm, the tool chain used to automate the optimization problem formulation and the fault-tolerant control system design. Experimental results and performance estimates from the conducted tests are described in section ñExperimental Results and Performance Estimationò.

BUILDING HVAC SYSTEM AND CONTROL-ORIENTED MODELS

This section describes the building HVAC system used for testing the control and diagnostics algorithm, its configuration, and the served zones. It also details some of the models used by the applied optimal control algorithm.

Description of the Building HVAC System

This section describes the main HVAC subsystems, their local control loops, and instrumentation. The HVAC system has a centralized architecture in which a steam-to-hot-water heat exchanger plant serves multiple AHUs in two identical large-size buildings located at the Navy Recruit Training Center, Great Lakes, IL. The HVAC systems consist of three Air Handling Units (AHU) serving 57 Variable Air Volume (VAV) units. Each of these AHUs serve 18 VAV units located in 9 compartments, each with a capacity level adequate to meet the load of several tens of occupants, which are occupied during night-time. The temperature set point is

based on a circadian variation, with higher set points (during cooling season) during night-time. This schedule is programmed in the BAS and is identical for all zones; there are not thermostats in the zones.

The focus of this effort in on AHUs and their VAVs which are instrumented as detailed in Table 1. Schematically illustrated in Figure 1, the local control algorithms for each of the subsystems of Table 1 are based on Proportional-Integral (PI) algorithms and rules as described below:

- The VAV dampers and re-heat coil valves are controlled based on two coordinated PI algorithms and rules that are driven by the zone set point tracking error. The local controllers seek to maintain the zone temperature within comfort bands that change at pre-scheduled intervals, and repeat every 24 hours. The discharge air temperature to each zone is controlled in open-loop (due to a lack of discharge air temperature sensors for most of the units). The volumetric air flow rates are controlled by modulating the VAV dampers to meet the scheduled set point values.
- The AHU fan speeds are controlled in order to maintain the pressure set points scheduled in BAS. The by-pass face dampers and the heating coil valves are controlled based on loops that track a discharge air temperature set point. The OA damper is controlled to maintain a minimum Mixed Air Temperature (MAT) set point (during the heating season), which is coordinated with the freeze-protection control rule.

Control-Oriented Models

This section describes the models used for the MPC algorithm design. In view of the time-scale separation of the zone temperature dynamics (with a time response in the order of tens of minutes) and HVAC subsystems (with a time response at most a few minutes), the only dynamical model considered in this approach corresponds to the zone temperature dynamics. The following models are developed at steady-state: outdoor air fraction model; mixed air temperature model; AHU heating coil model; AHU total air flow rate model; AHU supply fan model; VAV re-heat coil model. All expressions considered in this model are polynomial in order to facilitate derivations of first and second order derivatives required for the optimization solver, as explained in section ñAutomated Optimization Problem Formulationò.

After testing several ARMAX models (Auto-Regressive Moving-Average with External Disturbance), the following nonlinear ARX model was selecting for representing the dynamics of the zone temperatures:

$$\begin{aligned} T_{S_i}(k+1) = {} & \alpha_1 T_{S_i}(k) + \alpha_2 T_{S_i}(k-1) + \alpha_3 T_{S_i}(k-2) \\ & + \beta_1 T_{OA}(k) + \beta_2 T_{OA}(k-1) + \gamma\ \dot{m}_{sa,S_i}(k)\left[T_{sa,S_i}(k) - T_{S_i}(k)\right] + d_{S_i} \end{aligned} \quad (1)$$

where we used the notation as defined in the section Nomenclature, the sampling time is 5 minutes, and parameters $\alpha_{S_i,1}, \alpha_{S_i,2}, \alpha_{S_i,3}, \beta_{S_i,1}, \beta_{S_i,2}, \gamma, d_{S_i}$ are identified using several measurement tests. A part of the measurements, which included sensor measurements for all space temperatures T_{S_i}, were generated from experiments designed with selected input profiles; another part was selected from historical data. The controlled test inputs are AHU heat coil valve position $v_{AHU,HC}$, the VAV re-heat coil valve positions $v_{VAV_i,HC}$, and the VAV supply air flow rates $\dot{m}_{sa,S_i}$. One such test of data is illustrated in Figure 2a. Although these tests were applied to all

three AHUs and their corresponding VAVs, a model was used to generate estimates of VAV discharge air temperatures $T_{sa,S_i}(k)$ for the VAVs that were not instrumented with these additional sensors. This model is described in this section. The ability of the models to predict zone temperature was subsequently evaluated using new sets of data. Such a set of data is illustrated for one zone in Figure 2b. All HVAC subsystem control-oriented models are determined at steady-state due to their faster time response (one order of magnitude) relative to the zone temperature dynamics. The HVAC subsystems, their models and main assumptions are included in Table 2 (using the notation described in the Nomenclature section). All the steady-state models of Table 2 have been calibrated and validated with multiple sets of data. The histograms of the validation errors, between model predictions and measurements, are illustrated in the plots of Figure 3. Constraints related to the length of this paper preclude inclusion of additional time series data and more detailed discussions of the assumptions and restrictions of these models.

FAULT DETECTION AND DIAGNOSTICS ALGORITHMS

This section describes the implemented FDD system which uses a data-driven methodology integrated with domain knowledge to detect and diagnose faults. The FDD tool-chain includes a data-driven, off-line step of learning the nominal behaviors and an on-line step of detecting off-nominal behaviors. Data-driven methodologies have several advantages, such as low-cost commissioning, scalability, adaptability to system variation/evolution, and limited requirement of domain knowledge. The selected data-driven method consists of a graphical-network-based

approach which allows encoding the background domain knowledge and physics-based understanding of the system, while allowing discovery of new relationships within data streams using structure learning algorithms.

The FDD tool-chain used in this project comprises of four main components:

Data acquisition. Data-driven methods require sufficient data in order to reliably model a complex system. Data sufficiency involves two major aspects: spanning the operating space, and statistically significant amount of data. Both historical data and functional tests have been used in order to generate enough data to model discrete graphical models for different building subsystems.

Data pre-processing. The two major steps are: data quality verification, and data abstraction for modeling. In the data quality verification step, sensor observations are checked for data ranges, rate of changes and communication reliability. In order to prepare data for discrete probabilistic graphical models, continuous sensor observations were discretized using various techniques including equal-width, equal frequency and Maximally Bijective Discretization (Sarkar *et al.*, 2013).

Model learning. The graphical structure of the FDD model is learned in an exclusively data-driven manner to discover relationships between variables inherent in the data. The structure is then validated against domain knowledge and physics based understanding of the system. Using a goodness-of-fit metric that is based on accuracy of prediction of selected critical variables, model parameters are adjusted to achieve a good fit. The model parameters are essentially conditional probability values that capture causal dependencies among different system variables. For example, as shown in plate 1 of Figure 4, a probabilistic graphical model was

constructed to capture the dependencies among relevant variables of a VAV system. As mentioned in Table 3, two actuators, namely VAV damper and hot water valve and two measured variables, namely airflow through the VAV and power extracted from hot water (calculated using temperature difference across the coil and airflow) were considered for VAV modeling. With this choice of variables, the model captures the effect of damper opening on airflow as well as the effects of hot water valve opening and air flow on the power extracted from hot water. These causal relationships are visualized using directed arrows originating from the driving variable and terminating at the affected variable. Also, the thickness of an arrow signifies the level of a causal dependency. For example, for VAV system it was found that the damper-airflow dependency is much stronger compared to the other dependencies learnt from data. This also implies that it is easier to detect small anomalies related to the damper actuator by observing the air flow measurement. In general, the graphical network model for FDD is used to analyze new validation data to generate an anomaly score quantifying the extent of departure from the nominal performance of variable, given the measurement of other related variables. Based on the anomaly scores and a suitably chosen threshold, faults can be detected in any variable of the FDD model. The flagged events were then verified against ground truth.

On-line detection. Probabilistic graphical models are built for each relevant building sub-system and their graphical representations are discussed and illustrated in Table 3 and Figure 4. The graphical network models were calibrated and validated using multiple sets of data generated by overriding the BAS commands. Figure 5 contains the results of a validation test for the FDD algorithm associated with the damper d_{OA}. In this case, a fault was seeded by overriding the damper command to 85% open, while the BAS command was only 40%. Using the sensor

information from several temperature sensors, the FDD algorithm detected correctly the seeded faults. A small delay in generating the fault flag is observed and implemented in the algorithm to ensure that the fault persists for some time before it is flagged, and therefore reduce potential false alarms. More experimental data sets are presented and discussed in section ñExperimental Results and Performance Estimationò.

FORMULATIONS AND IMPLEMENTATION OF MODEL PREDICTIVE AND FAULT-TOLERANT CONTROL ALGORITHMS

This section describes the MPC and FTC problems, the hierarchical control architecture in which they are implemented, and the automated tool chain employed for their formulation.

An MPC algorithm is implemented to generate optimal set points for the building HVAC subsystems in real time by searching for the most energy-efficient control input sequences subject to system constraints (thermal comfort, component performance) and disturbances (weather, internal loads), similarly to the implementation in (Bengea *et al.* 2014). The MPC algorithm is implemented at the supervisory level in a hierarchical architecture whose signal flow is illustrated in Figure 5.

The MPC formulation integrates in the same framework the control-oriented building-system performance and zone-temperature models described in Table 2, and operational and thermal comfort constraints. The algorithm is formulated as a deterministic optimization problem as described below, where we use the same notation as in section Nomenclature and all the models are described in section 2.2.

The problem is formulated separately for each AHU and served VAVs and spaces.

Objective cost:	$Min\sum_{t_0}^{t_f}\left\{\sum_{VAV_i}\left[P_{AHU,HC}+P_{AHU,SF}+P_{VAV_i,HC}+Penalty(T_{S_i},T_{S_i,UB},T_{S_i,LB})\right]\right\}$ (2)
Optimization variables (21 control inputs):	VAV air flow rates $\dot{m}_{VAV_i,SA}^{ref}$ and re-heat coil valve positions $v_{VAV_i,HC}$, AHU discharge air temperature $T_{AHU,DAT}^{ref}$, and damper positions d_{OA} and d_{MA}
Subject to: Equality constraints for AHU, VAVs, and zone temperatures from Table 2	
AHU inequality constraints:	$T_{AHU,DAT}^{ref} \le T_{AHU,DAT}^{\max}(T_{MA},\dot{m}_{SA,AHU})$ (3) $\dot{m}_{AHU,SA} \le \dot{m}_{AHU,SA}^{\max}$ (4) $d_{OA,\min} \le d_{OA} \le d_{OA,\max}, \quad 0 \le d_{MA} \le 1, \quad 0 \le v_{AHU,HC} \le 1$ (5)
VAV inequality constraints:	$\dot{m}_{VAV_i,SA} \le \dot{m}_{VAV_i,SA}^{\max}$ (6) $v_{VAV_i,HC,\min} \le v_{VAV_i,HC} \le v_{VAV_i,HC,\max}$ (7)

The lower and upper bounds $d_{OA,\min}$ and $d_{OA,\max}$ in constraints (5) are estimated in real-time by the FDD algorithm. The formulation guarantees existence of an optimal solution of the FTC

algorithm without additional modifications due to the formulation of comfort constraints and model. The comfort constraints are formulated as soft constraints via function $Penalty(T_{S_i}, T_{S_i,UB}, T_{S_i,LB})$ in (2), which penalizes the excursions of the zone temperature outside of the comfort band $[T_{S_i,LB}, T_{S_i,UB}]$ which is scheduled for each zone and is time-dependent. The soft-constraint formulation does not cause any infeasibility issues when the actuator constraints are updated. The models in Table 2 depend directly on actuator values, and hence the constraints on modeled variables are automatically updated when the actuator constraints change. The FTC formulation above leads to optimal performance for the following scenarios:

- When the system is healthy, with no faults detected by the FDD algorithm, the actuator lower and upper bounds in (5) are $d_{OA,\min} = 0$ and $d_{OA,\max} = 1$, the generated set points are guaranteed (with respect to the deterministic formulation) to minimize the objective criteria (2) while meeting all constraints. This is a standard Model Predictive Control formulation.
- When the system is not healthy and the FDD algorithm detects faults, the lower and upper bounds in (5) may be set such that $d_{OA,\min} > 0$ or $d_{OA,\max} < 1$, respectively, depending on the fault magnitudes, and two scenarios are possible. With mild faults, comfort may still be maintained, but with a higher energy consumption (relative to a healthy system, as expected). With severe faults (e.g. damper stuck at high value during heating season), the effect of various disturbances on the HVAC system may not be attenuated reulting in the possibility that thecomfort constraints will not be met.

The above optimization problem, where the time variable has been removed for convenience, is solved at 15 minute time intervals and consists of: updating the sensor measurements and

weather forecast; estimating temperature states; diagnosing component faults; generating optimized set-points for the entire four-hour prediction horizon; communicating the new set point values (only for the next sampling time) to BMS. This repeated calculation of set points ensures solution robustness and optimality by using the most recent measurements and outdoor temperature forecasts. The optimization problem formulation workflowð the process by which the above mathematical problem is converted into an optimization algorithmð is illustrated in Figure 6.

AUTOMATED OPTIMIZATION PROBLEM FORMULATION

The MPC algorithms formulated in the previous section were converted into optimization problems by using the Berkeley Library for Optimization Modeling (BLOM) (Kelman *et al*. 2013). BLOM bridges the gap between simulation-oriented tools (Simulink, Modelica, etc.) and optimization-oriented tools (Kallrath 2004, Soares *et al.* 2003). BLOM is based on a new formulation for representing linear and nonlinear mathematical functions that aims to address some of the limitations of simulation-oriented tools. This formulation allows for direct computation of closed form gradients, Jacobians, and Hessians. The initial model formulation interface is based on Simulink, and BLOM provides a set of Matlab functions which convert a Simulink model into an optimization problem using a specific representation format. This problem representation is then used in a compiled interface to an optimization solver such as IPOPT (Wächter *et al*. 2006). BLOM consists of three main parts. First, there is the Simulink front end, where a dynamic model is represented using built-in Simulink blocks and the BLOM library blocks. Second, a set of Matlab functions is used to convert a Simulink model into the

internal mathematical representation described in (Kelman *et al*. 2013). Lastly, this problem representation is used by an interface to an optimization solver such as IPOPT. The BLOM front end for Simulink includes (in addition to the regular Simulink blocks) inequality, cost function, and designation of variables as free optimization variables or set by a user.

As shown in Figure 6, first, a model is created in Simulink and validated using forward simulation. Second, the model is converted to an optimization problem and exported to a solver (IPOPT). Third, problem data is supplied and a solution is obtained. The third step is repeated, with a new state measurement every time step. For efficient online solution of a large nonlinear MPC optimization problem in real time, it is critical that the sparsity structure of both the spatial connectivity in the model and the temporal causality over the MPC prediction horizon are captured and represented in the optimization formulation. BLOM is designed using an efficient sparse nonlinear problem representation in order to capture this information from the system model in a way that the optimization solver can fully utilize.

Table 4 presents typical performance of the BLOM library with IPOPT solver for the MPC problem formulated in the previous section. We present the execution time of problem solution for various problem sizes. The table shows that even for very large problems with more than 10000 variables and constraints, the library achieves good performance and IPOPT converges quickly to a Karush-Kuhn-Tucker point of the constrained finite-time optimal control problem.

EXPERIMENTAL RESULTS AND PERFORMANCE ESTIMATION FOR THE MPC, FDD AND FTC ALGORITHMS

This section presents the performance estimates generated based on multiple test conducted from November 2012 to March 2013 for three AHUs. The performance results are described separately for the FDD, MPC and FTC algorithms. The section starts with a description of the method employed to estimate the overall system performance, then describes aggregated performance results, followed by plots of experimental data for the MPC, FDD and FTC algorithms and concludes with a discussion of the limitations of this performance analysis.

The main performance metrics addressed in this effort are: overall energy consumption, peak power, comfort, and percentage of faults identified correctly. The overall energy (power) consumption was calculated using both electrical energy (power) consumption for fans and thermal energy (power) consumption for heating heat exchangers. The overall energy (power) consumption was estimated by converting the thermal component to an electrical component using the estimated Coefficient of Performance (COP) of the heating plant. The comfort criteria was initially intended to be addressed as a hard constraint (as a band around zone thermostat set points), but it was observed that the baseline control algorithms did not meet this constraint for several time intervals every day. Therefore a more realistic criteria was used that estimates comfort violations (during the heating season) as

$$\int_{t_0}^{t_f} \max(0, T_{S_i,LB}(t) - T_{S_i}(t))dt \tag{8}$$

which represents the accumulated time interval over which the comfort constraint is not met (during the heating season) weighted by the level of constraint violation. The value of the integral (8) calculated over various test time intervals represents the discomfort level.

In the following sections, we first discuss the results pertaining to the MPC algorithm (energy consumption, peak power reduction, and discomfort reduction), then the performance of the FDD algorithm, and lastly performance of the FTC algorithm. The results of the test are grouped and compared based on the health status, the type of the executed algorithm and the criteria for data selection. This information is presented in Table 5.

Performance Results for the Model Predictive Control Algorithm for Healthy HVAC System

We present first the overall results generated based on the sensor and meter data recorded from the demonstrations conducted during the heating season 2012-13. The overall results, pertaining to Set I in Table 5, are illustrated in Figure 7 for each AHU, relative to the baseline BAS schedule performance; the performance targets are illustrated as horizontal red lines. For each AHU_i, $i = 1,2,3$, the results in Figure 7 pertaining to energy savings, peak power reduction, and thermal discomfort are generated by averaging its performance over all demonstration days using the following formula:

$$PerfMetric\ (AHU_i) = \frac{1}{N_{AHU_i,MPC}} \sum_{MPC_j} \left[\frac{1}{N_{AHU_i,Baseline}} \sum_{Baseline_k} \left(1 - \frac{PerfMetric\ (AHU_i, MPC_j)}{PerfMetric\ (AHU_i, Baseline_k)} \right) \right] \quad (9)$$

The performance metrics in (9) represent the calculation of two averages: the first is across all MPC algorithm demonstration days, MPC_j, and the second is for all the baseline days $Baseline_k$ (during which the HVAC system is controlled by the baseline algorithm) that are selected to be

compared against the performance results generated in MPC_j demonstration day. This selection is discussed next.

Due to a lack of sufficiently large sets of test data, a selection criteria is required to identify specific baseline days and MPC demonstration days for conducting performance analysis. The criteria selected for this analysis is based on ambient temperature; this selection was based on the assumption that, in lack of occupancy data, as is the case with many demonstration sites, the ambient conditions generate the largest disturbances that have to be rejected by HVAC system. Such a selection is illustrated in Figure 8 (left) where the ambient-temperature time series data for one MPC day and the corresponding baseline days are plotted.

The same figure also illustrates (right plot) the zone temperatures generated with the corresponding algorithms during the same days as selected in the left plot. The performance of the MPC algorithm and the baseline algorithms during these days is further detailed in Figure 9 which illustrates that the baseline algorithms did not meet comfort constraints when the set point values were changed (according to the circadian schedule implemented in BAS). In order to meet these constraints, when the set point value is increased (during heating season) the MPC algorithmôs peak power value exceeded the baseline algorithmôs peak power values.

The bar graphs in Figure 10 and 11 further illustrate a subset of the test data that was used to calculate the performance metrics (using (9) and three baseline days with closest ambient temperature values for each MPC day) of Figure 7. Energy consumption and peak power reduction levels are illustrated in Figure 10, where negative values in the peak power bar graph mean that MPC algorithm used higher power levels. The mean zone CO_2 levels and comfort violations are illustrated in Figure 11.

Performance Results for the Fault Detection and Diagnostics Algorithm

The overall FDD algorithm performance was estimated using sensor and meter data recorded during multiple test windows, grouped as Set II in Table 5. Based on this data, it was estimated that the FDD algorithm correctly diagnosed the HVAC subsystem faults in 84% of the cases (level illustrated in Figure 7), missed the detection of 6% of the events, and generated false alarms in 10% of the total events which consist of equal number of seeded and non-seeded (real) faults. The seeded faults were implemented by overriding the commands communicated by the controllers (with the BACNet message priority set at a value that enables the override), without communicating these overrides to the FDD algorithm. An example of a correctly diagnosed damper fault is illustrated in Figure 17 where the trained VAV FDD algorithms correctly diagnosed the damper-stuck faults. This existence of these particular faults was confirmed by investigating the actual VAVs.

The lack of sufficient instrumentation and the inaccuracy of sensors for building HVAC systems present significant challenges that result occasionally in miss-detection or false positive classifications. Particularly for high capacity HVAC units, with large air duct diameters, the inaccuracies of air temperature sensors at different location can result in false positive FDD outcomes. A few example data sets are presented in Figure 18, where the following sensing inconsistencies are observed: (i) when d_{OA} closes, T_{MA} increases and gets closer to T_{RA} as expected, but there are also time intervals over which T_{MA} exceeds T_{RA}; (ii) T_{MA} exceeds T_{HR} when d_{OA} is fully open; (iii) T_{MA} exceeds T_{HR} and T_{RA} (which have similar values) by about 5^0F. In all these cases, the FDD algorithm can trigger false alarms on some time sub-intervals. In such cases, with the limited sensor set data FDD algorithms cannot distinguish among multiple cases:

mis-calibrated sensors; leakages that depend nonlinearly on damper positions; non-mixed air flows with non-uniform temperatures. In view of these limitations, the outdoor air damper faults that are seeded correspond to large variations in d_{OA} in the interval [30%, 70%] opening; where the lower bound is imposed by fresh air constraints, and the upper bound was selected to avoid case (ii) discussed above. With this limited range on the outdoor air damper seeded-faults, which minimize the rate of false alarms for this damper, the false alarms are mostly generated for cases when large transient conditions (due to large changes in set point values) occur in the system.

Performance Results for the Fault-Tolerant Control Algorithm

This section presents the results that pertain to Sets III and IV of Table 5 which were generated by comparing the performance of the FTC algorithm against the performance of the BMSôs control logic and nominal MPC algorithms, respectively.

The FTC algorithm was implemented as described in section ñFormulations and Implementations of Model Predictive and Fault-Tolerant Control Algorithmsò. The seeded fault is associated with the OAD damper, which was identified to have the largest impact on the HVAC system energy consumption among all the considered actuator subset. In order to generate the faults in a controlled environment, the BASôs OAD command was overriden, over two time intervals illustrated in Figure 12. First the OAD command is overriden with the stuck-fault values, at 30% and 60%, respectively, for the two test intervals, which correspond to Sets III and IV of Table 6. The FDD algorithm generates a signal (colored blue in the mentioned figure) that represents a mismatch between the predicted, model-based and measured OAT values. When the magnitude of this signal exceeds a certain threshold, a fault flag is generated which triggers the fault isolation and characterisation algorithm. The detected OAD fault is used

by the FTC algorithm to update its constraints $d_{OA,\min} > 0$ and $d_{OA,\max} < 1$, which are used to generate new values of the DAT set points as illustrated in Figure 12 (right). A direct consequence of the OAD being stuck at large values during the heating season was that large values of DAS are no longer feasible; therefore the DAT set point values had to be decreased during the fault-seeing time intervals. The performance data described in this section pertains to these two time intervals.

The performance data associated with tests of Set III in Table 5 is illustrated in Figures 13 and 14. In this test the baseline BMSôs control logic, which does not have an explicit fault-accommodation logic, is compared against the performance of the FTC algorithm. As illustrated in the mentioned figures, the FTC algorithms meets the comfort constraints while also reducing energy consumption. This is possible because the FTC algorithm reuses more indoor air, as illustrated by the higher CO_2 levels.

The performance data associated with tests of Set IV in Table 5 is illustrated in Figures 15 and 16. The MPC algorithm was executed for the healthy HVAC system, for which no faults were seeded. The comparison provides insights into the impact of the fault on optimal control algorithm performance. To meet the comfort constraints, the FTC algorithm consumed significantly more energy with a higher peak power than the MPC algorithm. In spite of the fact that the OAD values were higher for the FTC algorithm, the CO_2 levels are similar for both algorithms, which can only be partially explained by the different occupancy levels in the spaces served during these tests. However, these levels cannot be estimated due to lack of occupancy sensors.

Limitations of the Performance Estimation Method

There are several limitations in the calculation of the performance estimates of the FDD and MPC algorithms. The limitations are reviewed and discussed below for each algorithm.

For the FDD algorithm these limitations are consequences of the following factors:

- Only single faults are considered in this effort, and they are exclusively assigned to actuator faults. Except for these faults, the HVAC units were considered otherwise healthy. As previously mentioned, it is not possible to distinguish between all possible faults that can occur with a limited sensor and meter data set.
- HVAC control systems have a large degree of fault-accommodation without explicitly estimating any faults. An example is the discharge air temperature control loop at the AHU level which controls the volume flow rate of the mixed airflow through the heating coil deck and the heating valve position. A large number of combinations between the flow rate and the heating valve positions can lead to the same temperature differences between the mixed air and discharged air. Without intermediate sensors for measuring the inlet temperature to the heat exchanger, an FDD algorithm has limited information for detecting any faults associated with these two actuators when using only data generated with the local controllers.
- The FDD performance reported in Figure 8 corresponds only to the units that were instrumented with additional sensors (as described in Table 1).

The estimation of the uncertainty magnitude in the reported performance levels of the MPC algorithm is limited by factors related to sensor instrumentation and test data size:

- Although the performance levels are estimated using measurement data from 26 days distributed unevenly during the entire heating season 2012-13, it is unclear whether the

distribution of the internal loads and ambient conditions was representative for all heating seasons in the selected buildings. The level of sensor instrumentation needed to generate these estimates is beyond the level of instrumentation in standard commercial buildings, such as those used for demonstration to support this effort. Therefore an extrapolation of the results in Figure 7 to other heating seasons, ambient conditions, or usage patterns cannot be made directly. We note, however, that large levels of energy savings were also demonstrated for a smaller AHU, in similar ambient conditions, and different HVAC configuration and usage patterns (Bengea *et al.* 2014).

- The method used for MPC performance estimation is based on the assumption that the largest disturbance is ambient temperature, and therefore similarity in the outdoor air temperature patterns is the most important criteria when selecting multiple sets of days for performing energy consumption comparisons. When sufficiently large sets of data are available, using multiple criteria would increase the accuracy of the performance estimates.
- Less than 30% of the models are validated. Due to limited sensor instrumentation for two of the AHUs (ñB4 AHU2ò and ñB3 AHU1ò in Figure 7), the AHU and VAV heat exchanger models could not be validated. Therefore the VAV re-heat coil energy consumption for these AHUs were estimated using the same models as those used for the AHU for which additional sensors were instrumented (as described in Table 1).
- The MPC algorithm does not use zone occupancy models and therefore does not control directly the CO_2 levels in the zones. The MPC algorithm met the minimum outdoor air damper constraint (designed for the baseline algorithm to meet the fresh air requirements). However, after the demonstrations it was observed that the MPC algorithm consistently

increased this level in all zones by about 35% on average (across all zones served by all three AHUs). The limitations in the sensor and meter data prevent detailed estimation of specific portions of the reported energy consumption levels in Figure 7 that are due to decreasing the outdoor air damper position (while still meeting the minimum damper-position constraint), meeting different occupancy loads, and increasing thermal comfort.

CONCLUSIONS

The paper presents the design, implementation, and performance results of two model-based algorithms based on tests conducted in two large-size commercial buildings during the heating season 2012-13. The MPC algorithm uses sensor data to generate periodic updates of AHU and VAV unit set point values that reduce energy consumption while maintaining all zones temperatures within a comfort band. The FDD algorithm uses sensor and meter data to isolate on-line faults associated with the AHU actuators. The individual performance benefits of the two algorithms are estimated based on test results compared against historical baseline data generated during test periods with similar ambient conditions. Although the energy performance depends on uncertainties which cannot be completely characterized with limited data, the results demonstrate the potential of the algorithms to reduce energy levels to levels that provide favorable cost benefits.

ACKNOWLEDGMENT

We also thank Mr. Peter Behrens, energy manager at naval station great lakes, for his support in conducting the demonstrations. Views, opinions, and/or findings contained in this report are those of the authors and should not be construed as an official department of defense position or decision unless so designated by other official documentation.

FUNDING

This material is based upon work supported by the Humphreyôs Engineer Support Activity under Contract No. W912HQ-11-C-0016. The authors are grateful for the financial support and guidance provided by the SERDP/ESTCP Office under the leadership of Drs. Jeff Marqusee and Jim Galvin.

NOMENCLATURE AND MATHEMATICAL NOTATION

AHU	Air Handling Unit
APAR	AHU Performance Assessment Rules
BLOM	Berkeley Library for Optimization Modeling
BMS	Building Management System
CFM	Cubic Feet per Minute
CO_2	Carbon Dioxide
DAS	Discharge Air Set point
FBD	Face Bypass Damper
FDD	Fault Detection and Diagnosis
FTC	Fault-Tolerant Control
GPM	Gallon per Minute
HCV	Heating Coil Valve
HR	Heat Recovery
HVAC	Heating, Ventilation and Air Conditioning
MPC	Model Predictive Control
NOAA	National Oceanic and Atmospheric Administration
VAV	Variable Air Volume
VFD	Variable Frequency Drive

$\dot{m}_{sa,S_i}$ and T_{sa,S_i}	Mass flow rate and temperature of supplied air to space S_i
T_{OA}, T_{MA}, T_{RA}	Temperatures of Outdoor Air (OA), Mixed Air (MA), and Return Air (RA), respectively
T_{S_i}, T_{UB,S_i}, T_{LB,S_i}	Air temperature in space S_i and upper and lower bounds of the temperature comfort band for space S_i
d_{OA}, d_{MA}, d_{RA}, d_{FBD}	Damper positions for Outdoor Air (OA), Mixed Air (MA), Return Air (RA), and by-pass air flow streams, respectively
$T_{sa,AHU}$, T_{HD} T_{CD}	Temperature of air supplied by AHU (downstream of hot and cold decks; upstream of VAV units); Temperature air discharged at the outlet of the hot and cold decks, respectively
f_{OA}	Ratio between mass flow rate of outdoor air flow and mass flow rate of the mixed air flow
$v_{AHU,HC}$, $v_{VAV,HC}$	Normalized position of the heating coil valve (the subscript makes it clear whether this belongs to the AHU heating coil of VAV re-heat coil
P	Power (thermal or electrical)
T_{SP,S_i}	Set point for space S_i

REFERENCES

Adetola, V., Ahuja, S., Bailey, T., Dong, B., Khawaja, T., Luo, D., OõNeil, Z., Shashanka, M., 2013, ñScalable Deployment of Advanced Building Energy Management Systemsò, ESTCP-EW-1015 Project, Technical Report.

Atanu Talukdar & Amit Patra. Dynamic Model-Based Fault Tolerant Control of Variable Air Volume Air Conditioning System. HVAC&R Research Vol 16 (2), 2010. Pgs 233-254

Baotic, M., F. Borrelli, A. Bemporad, and M. Morari. ñEfficient on-line computation of constrained optimal controlò. SIAM Journal on Control and Optimization, 5:2470ï2489, September 2008

Bengea, S., Kelman, A., Borrelli, F., Taylor, R., and Narayanan, S., 2014, ñImplementation of model predictive control for an HVAC system in mid-size commercial buildingò, Journal of HVAC & R Research, Volume 20, Issue 1, pp. 121-135, 2014.

Bengea, S., Li, P., Sarkar, S., Vichik, S., Adetola, V., Kang, K., Lovett, T., Leonardi, F., Kelman, A., ñModel Predictive Control and Fault Detection and Diagnostics of a Building Heating, Ventilation, and Air Conditioningò, 3rd International High Performance Buildings Conference at Purdue, July 14-17, 2014, West Lafayette, IN.

Borrelli, F., J. Pekar, M. Baotic and G. Stewart. ñOn The Computation Of Linear Model Predictive Control Lawsò. Automatica, 46(6):1035-1041, June 2010.

Borrelli, F., ñConstrained Optimal Control of Linear and Hybrid Systemsò, Lecture Notes in Control and Information Sciences, vol. 290. Springer, 2003.

Bourassa, N., Automatic Diagnosis for Ailing Rooftop Air Conditioners, PIER Technical Brief, July 2005.

Brand, M.E., Pattern Discovery via Entropy Minimization. In Uncertainty 99: AISTATS 99, 1999.

Brand, M.E., Structure Learning in Conditional Probability Models via an Entropic Prior and Parameter Extinction in Neural Computation Journal, Vol. 11,No. 5, pp. 1155-1182, July 1999.

Chiang, L., E. Russell, R. Braatz, Fault Detection and Diagnosis in Industrial Systems, Springer Verlag, London, 2000.

Dudley, J.H., Black, D., Apte, M., Piette, M.A. and Berkeley, P. 2010. Comparison of Demand Response Performacnr with an EnergyPlus Model in a Low Energy Campus Building. 2010 ACEEE Summer Study on Energy Efficiency in Buildings. Pacific Grove, CA. August 15-20, 2010.

Environmental Protection Agency, 2008, Report on Environment, Final Report EPA/600/R-07/045F. United States Environmental Protection Agency.

Fernandez, N., Brambley, M. R., and Katipamula, S., Self-Correcting HVAC Controls: Algorithm for sensors and Henze, G., D. Kalz, C. Felsmann, and G. Knabe. 2004. ñImpact of forecasting accuracy on predictive optimal control of active and passive building thermal storage inventory.ò HVAC&R Research, Vol. 10, No. 2, pp. 153ï 177.dampers in air handling units, US DOE report 2009 (Contract DE-AC05-76RL01830).

Henze, G.P., Kalz, D. E., Liu, S., and Felsmann, C., Experimental Analysis of Model-Based Predictive Optimal Control, HVAC&R Research, Vol. 11, No. 2, 2005, pp. 189-213.

Kallrath, J., Modeling Languages in Mathematical Optimization, ser. Applied Optimization. Kluwer Academic Publishers, 2004.

Kelly, G. 1988. ñControl system simulation in North Americaò. Energy and Buildings Vol. 10, pp. 193ï 202.

Kelman, A., Vichik, S., Borrelli, F., ñBLOM: The Berkeley Library for Optimization Modeling and Nonlinear Predictive Controlò, Internal report, Department of Mechanical Engineering, University of California, Berkeley, 2013. Website: http://www.mpc.berkeley.edu/software/blom

Li, P., Baric, M., Narayanan, S., and Yuan, S. 2012, A Simulation-Based Study of Model Predictive Control in a Medium-Sized Commercial Building, *2nd International High Performance Buildings Conference at Purdue*, July 16-19, 2012, West Lafayette, IN.

Li, P., Li, D., Vrabie, D., Bengea, S., Mijanovic, S., 2014, Experimental Demonstration of Model Predictive Control in a Medium-Sized Commercial Building, 3rd International High Performance Buildings Conference at Purdue, July 14-17, 2014, West Lafayette, IN.

Ljung, L., ñSystem Identification: Theory for the Userò, Prentice Hall.

Ma, Y., Borrelli, F., Hencey, B., Coffey, B., Bengea, S., Packard, A., Haves, P., ñModel Predictive Control for the Operation of Building Cooling Systemsò, in Proceedings of the American Control Conference, July 2010, Baltimore, MD.

Mayne, D., J. Rawlings, C. Rao, and P. Scokaert. 2000. ñConstrained model predictive control: stability and optimality,ò Automatica, Vol. 36, No. 6, pp. 789ï 814.

Morari, M. and J. Lee. 1999. ñModel predictive control: past, present and future,ò Computers and Chemical Engineering, Vol. 23, pp. 667ï 682.

Piette, M.A.,S. Kinney, and P. Haves. Analysis of an Information Monitoring and Diagnostic System to Improve Building Operations, Energy and Buildings 33 (8) (2001), 783-791.

Radhakrishann, R., D. Nikovski, K. Peker, and A. Divakaran. Locally Weighted Regression for Fault Detection and Diagnosis of HVAC Equipmentò, IEEE Intl. Conf. on Industrial Electronics, 2006.

Roth, K. W., Westphalen, D., Feng, M. Y., Llana, P., and Quartararo, L. (2005). ñEnergy impact of commercial building controls and performance diagnostics: market characterization, energy impact of building faults and energy savings potentialò. Report prepared for U.S. Department of Energy. TIAX LCC, Cambridge, MA. http://www.epa.gov/cleanenergy/energy-resources/refs.html

Sarkar, S., A. Srivastav, and M. Shashanka, ñMaximally Bijective Discretization for Data-driven Modeling of Complex Systemsò, Proceedings of American Control Conference, (Washington, D.C.), 2013

Siroky J, Oldewurtel F, Cigler J, Privara S. 2011, ñExperimental analysis of model predictive control for an energy efficient building heating systemò. Appl Energy. Vol. 88, pp. 3079ï 3087.

Soares R. d. P. and A. Secchi, European Symposium on Computer Aided Process Engineering-13, 36th European Symposium of the Working Party on Computer Aided Process Engineering, ser. Computer Aided Chemical Engineering. Elsevier, 2003, vol. 14. [Online]. Available: http://www.sciencedirect.com/science/article/pii/S1570794603802390

Wächter and L. T. Biegler, ñOn the Implementation of a Primal-Dual Interior Point Filter Line Search Algorithm for Large-Scale Nonlinear Programmingò, Mathematical Programming 106(1), pp. 25-57, 2006.

Table 1. Instrumentation of the HVAC System			
	AHU Instrumentation	**VAV Instrumentation**	**Spaces**
Common sensors (baseline installation)	• Discharge air ,mixed air , and return air temperature sensors; damper and valve position sensors • Fan VFD speed and power meter	• Volumetric air flow rate metering station • Re-heat coil valve position sensor	• Zone temperature, CO_2 sensors
Special sensors instrumented for this effort	• One AHU was instrumented with BTU meters for both heating and cooling coils, and volumetric air flow rate metering station • The same AHU was instrumented with more accurate averaging mixed and discharge temperature sensors • Forecast of outdoor air temperature (downloaded on-line from NOAA)	• Three VAVs have been instrumented with BTU meters, inlet air temperature sensors, re-heat coil valve position sensors, and damper position sensors • 18 VAVs have been instrumented with discharge air temperature sensors	• Zone relative humidity sensors
Common actuators	• Dampers: face by-pass dampers, which control the mixed air flow portion that passes through the heating deck • Heating and cooling coil valves	• Dampers • Re-heat coil valves,	

Table 2. HVAC Steady-State Models and Assumptions		
HVAC Subsystems	**Assumptions**	**Equations**
Outdoor air fraction and mixed-air temperature	• Steady-state models as functions of outdoor air damper, specifically for heating season	$f_{OA} = c_{2,OA} \cdot d_{OA}^2 + c_{1,OA} \cdot d_{OA} + c_{0,OA}$ $T_{MA} = f_{OA} \cdot T_{OA} + (1 - f_{OA}) \cdot T_{RA}$
Thermal power of AHU heating coil	• Steady-state models as functions of volumetric air flow rate, inlet and discharge air temperatures	$P_{HC} = \dot{m}_{SA} \cdot c_{pa} \cdot (T_{DA,AHU} - T_{MA} - \Delta T_{SF})$
AHU supply air flow rate	• Constant air flow leakages in the supply ducts to zone VAVs	$\dot{m}_{SA,AHU} = c_{1,SA} \cdot \sum_i \dot{m}_{SA,VAV_i} + c_{0,SA}$
Electrical power of supply fan	• Function of supplied air flow	$P_{SF} = c_{3,SF} \cdot \dot{m}_{SA,AHU}^3 + c_{2,SF} \cdot \dot{m}_{SA,AHU}^2 + c_{1,SF} \cdot \dot{m}_{SA,AHU} + c_{0,SF}$
Thermal power of VAV re-heat coils	• Steady-state models as functions of volumetric air flow rate, inlet and discharge air temperatures	$T_{SA,VAV} = T_{SA,AHU} + c_{3,VAV} \cdot \frac{T_{W,HC,in}}{\dot{m}_{SA,VAV}^{c_{2,VAV}}} \cdot v_{HC}^{c_{1,VAV}}$

Table 3. FDD approach details corresponding to the AHU subsystems		
Subsystem	**Faults**	**FDD graphical model nodes**
VAV terminal unit	• Damper d_{VAV_i} : stuck; air leakages; sticky • Valve $v_{VAV_i,HC}$: stuck; leakages; sticky	Damper position, supply air flow rate, heating coil valve position, and air flow thermal power
AHU	• Damper d_{OA} : stuck; air leakages; sticky	Damper position, estimated outdoor-air flow fraction (based on temperature measurements)
	• Valve $v_{AHU,HC}$: stuck; water leakages; sticky	Heating coil valve position, air flow thermal power, air flow rate, face by-pass damper position, difference between inlet and outlet water temperatures
	• Fan: capacity and efficiency changes	Fan speed, electrical power, supply static pressure, air flow rate

Table 4. BLOM execution results			
Prediction horizon length (steps)	**20**	**30**	**50**
Number of variables in solver	11180	16770	27950
Number of constraints	8777	13252	22202
Non-zeros in Jacobian and Hessian	31682	48227	81317
Number of solver iterations	91	142	128
Total solution time [sec]	6.6	20.3	46.8
Time spent in BLOM callbacks	34%	30%	29%

Table 5. Test data, algorithms and criteria for data selection				
Test data	**Healthy HVAC System**	**Faulty HVAC System**	**Test Data Conditions and Selection Criteria**	**Objective**
Set I	• Baseline Control Logic • MPC algorithm		Similar OAT time series data patterns for historical HVAC baseline data as for the conducted MPC tests.	MPC algorithm performance estimation
Set II		• Baseline Control Logic • FDD algorithm	Faults seeded by overriding the BASôs OAD commands.	FDD algorithm performance estimation
Set III		• Baseline control logic • FTC algorithm	Executed simultaneoulsy, during same ambeint conditions, on two different, similar AHUs serving similar spaces	Estimate benefits fo FTC algorithm
Set IV	MPC algorithm	FTC algorithm	Executed simultaneoulsy, during same ambeint conditions, on two different, similar AHUs serving similar spaces	Estimates benefits of fault-tolerance for MPC algortihm

Table 6. Demonstration conditions for the FTC algorithm (Sets III and IV of Table 5)			
Test Days	**Fault Injection**	**Demo Time Period**	**Mean Outdoor Air Temperature (◦F)**
Day 1	Outdoor air damper stuck at 30%	9am - 15pm	27.2
Day 2	Outdoor air damper stuck at 60%	8:30am - 17pm	37.4

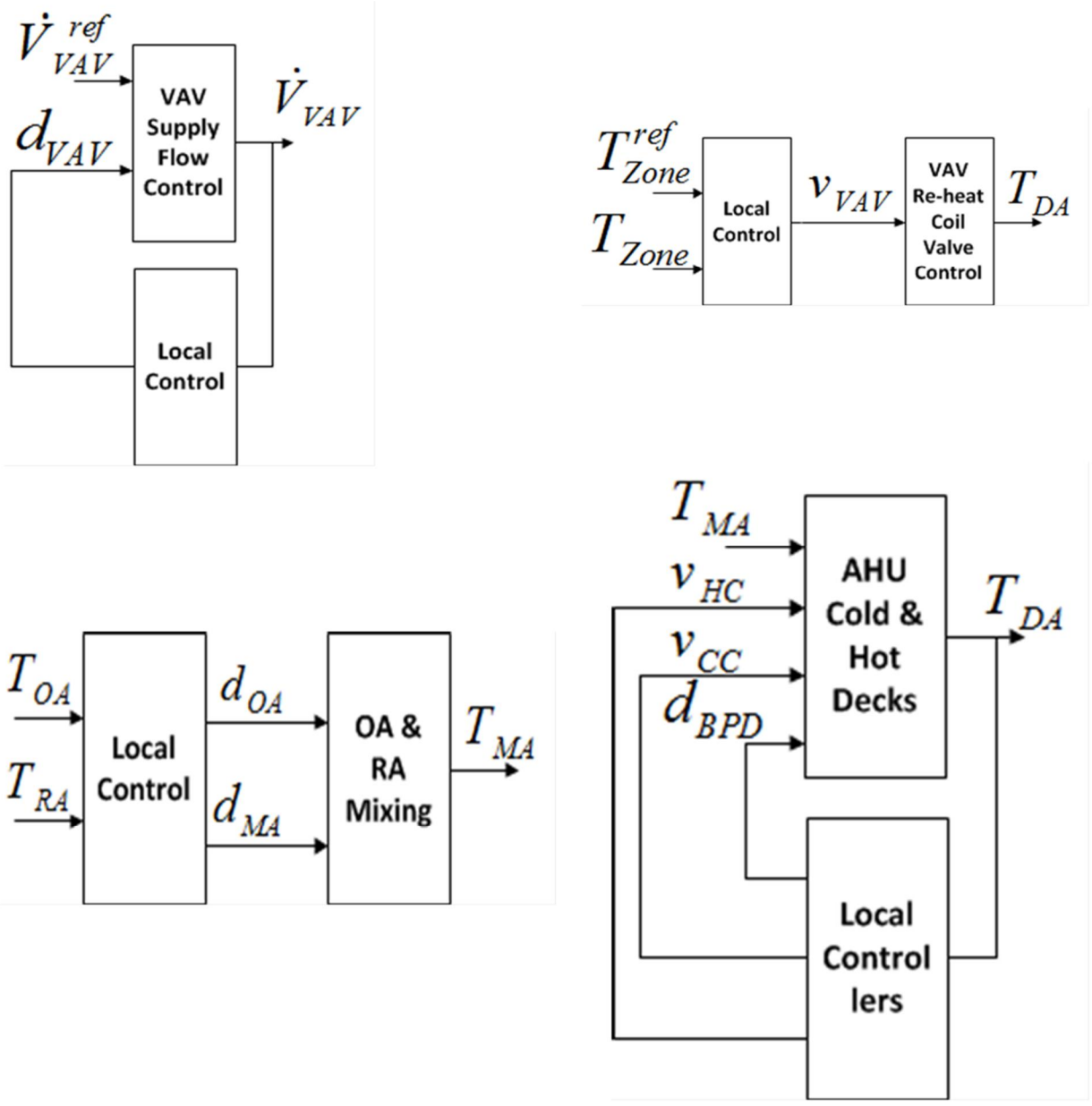

Figure 1. Signal flows of the VAV local control loops corresponding to supply air flow rate and zone temperature (top two figures); Signal flows of the AHU local control loops corresponding to mixed air and discharge air temperatures (bottom two figures)

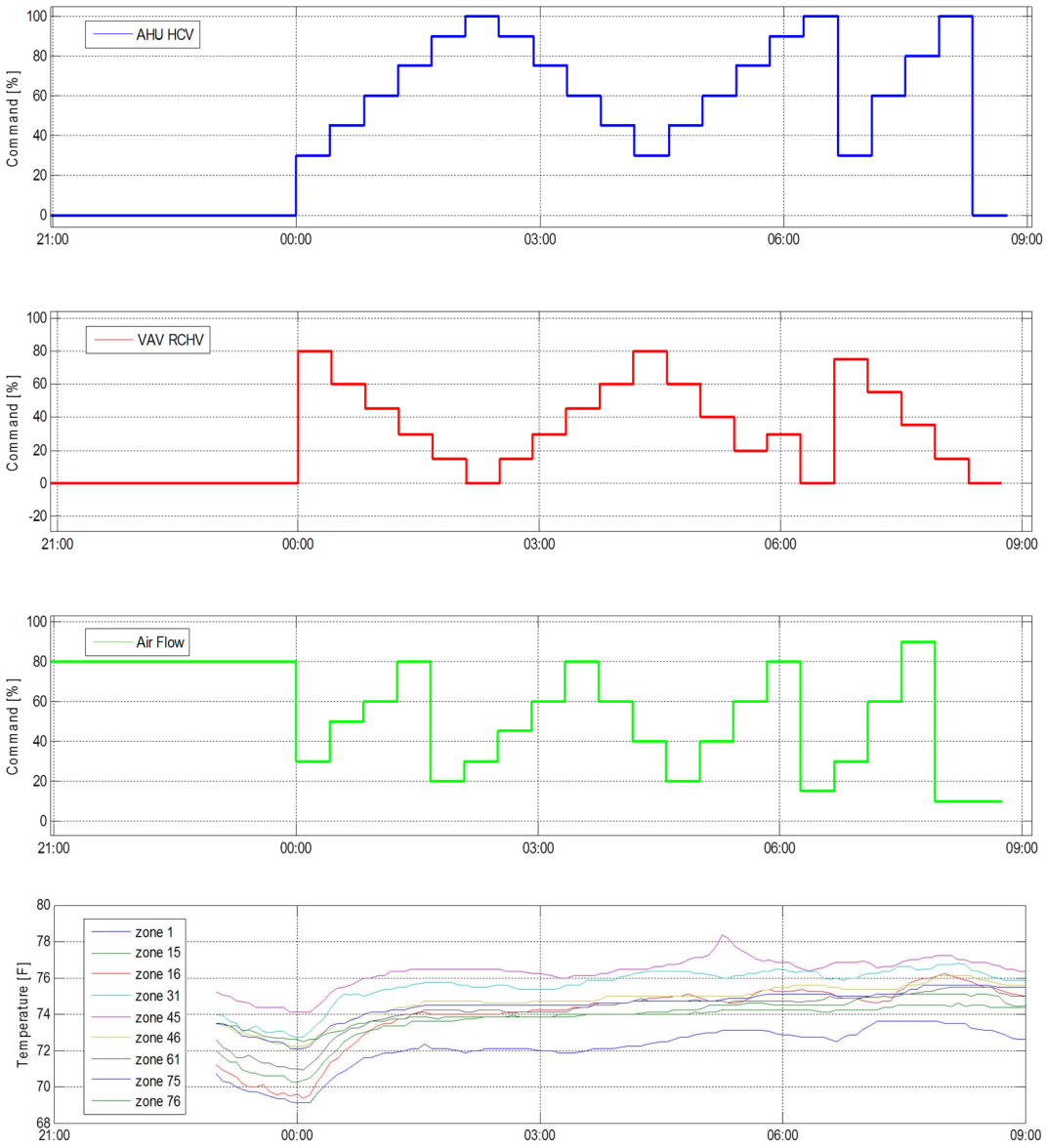

Figure 2a. Normalized time series data of the inputs $v_{AHU,HC}$, $v_{VAV_i,HC}$, and $\dot{m}_{sa,S_i}$ for a system identification test for AHU1 (top three figures), and corresponding zone temperatures measurements (bottom figure)

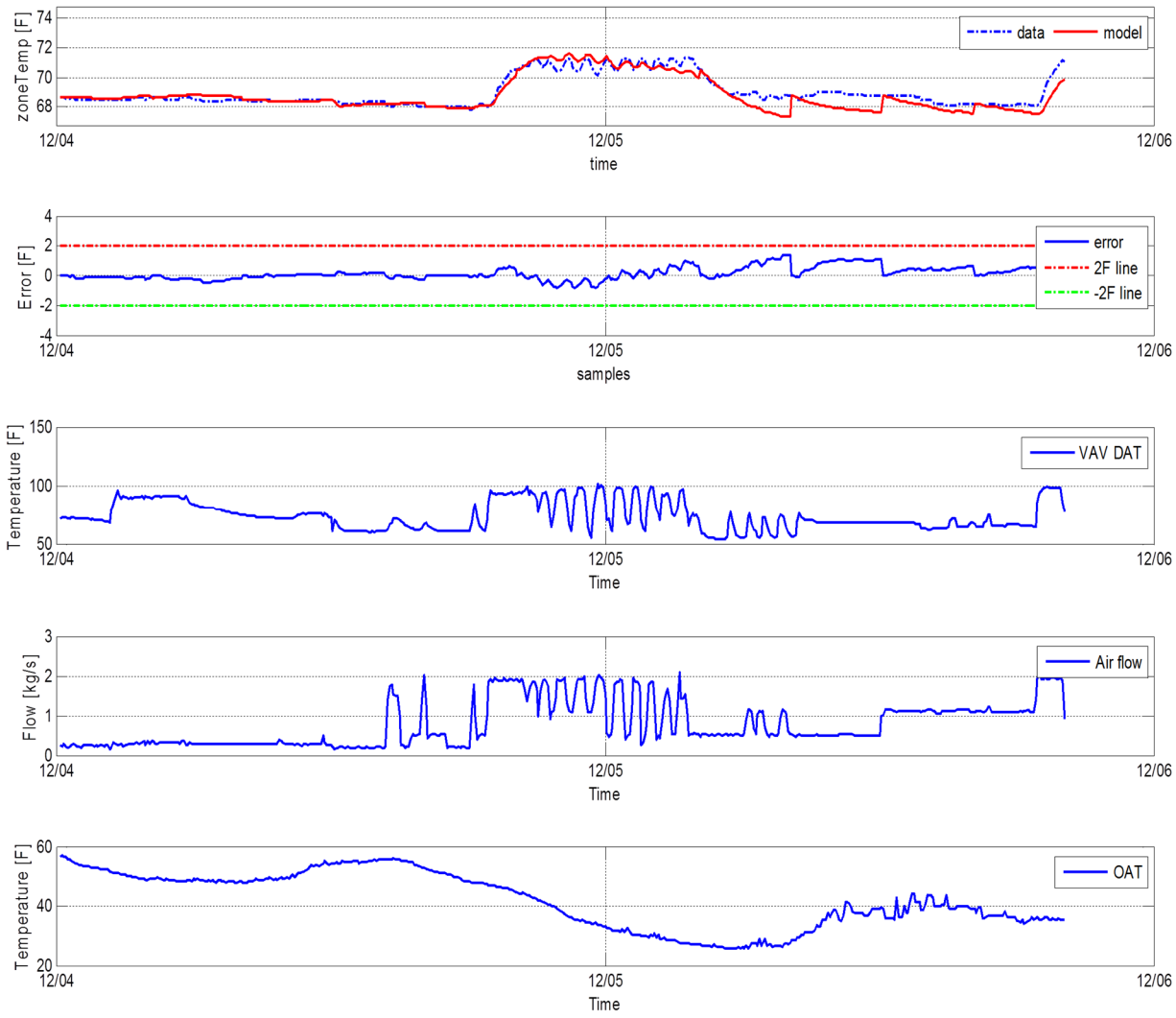

Figure 2b. Model validation results using new data sets based on which it was concluded that the zone temperature modeling error is smaller than 2deg F

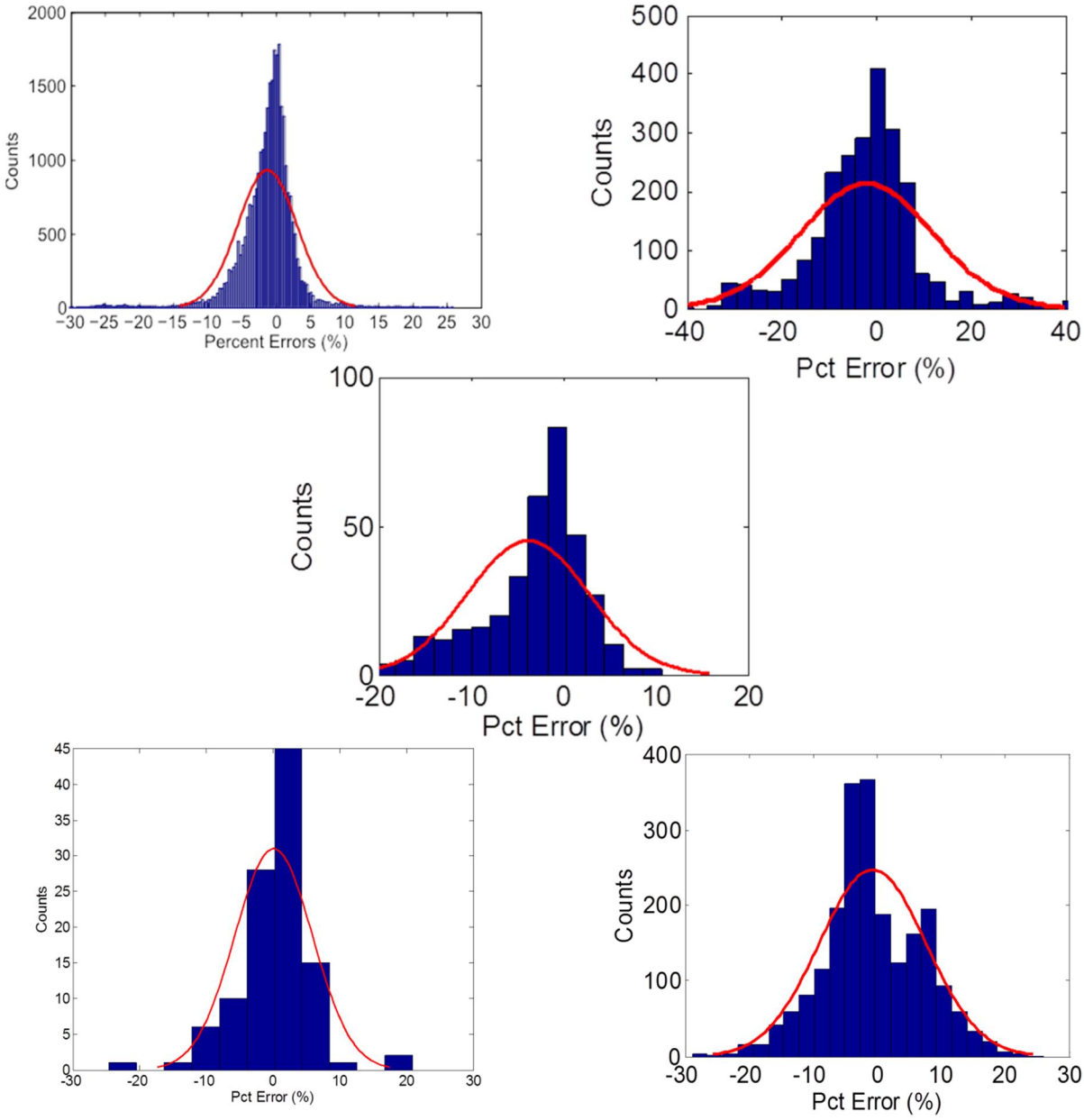

Figure 3. Histograms of the validation errors for all models of Table 2 (in the same order as in the table: mixed-air temperature; AHU heating coil thermal power; AHU supply air flow rate; AHU supply fan power; VAV re-heat coil thermal power)

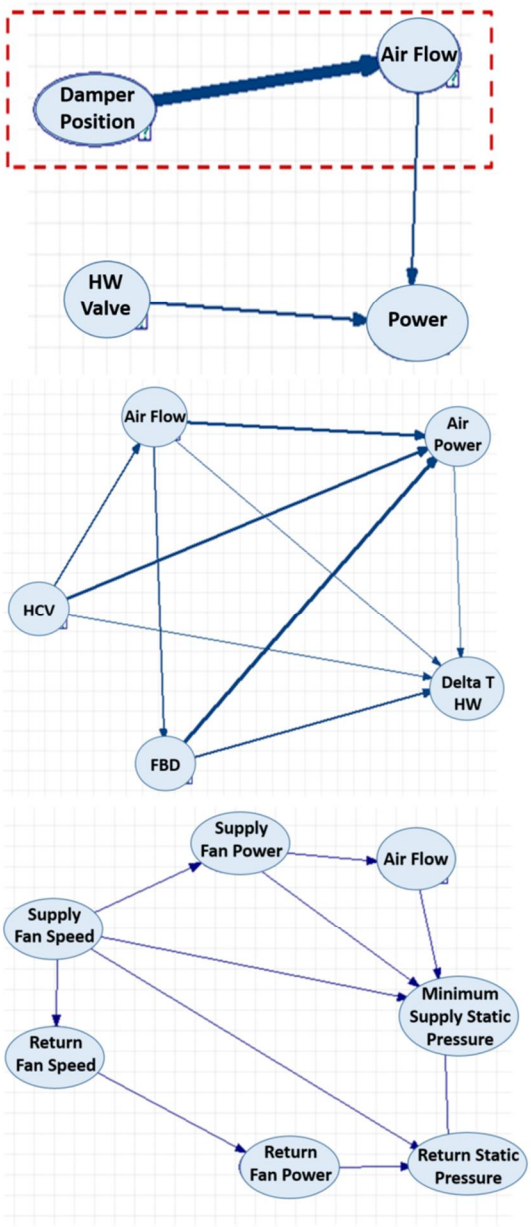

Figure 4. Graphical FDD models for the HVAC actuation subsystems: Variable Area Volume unit (left); AHU heating coil (middle); AHU fans (right)

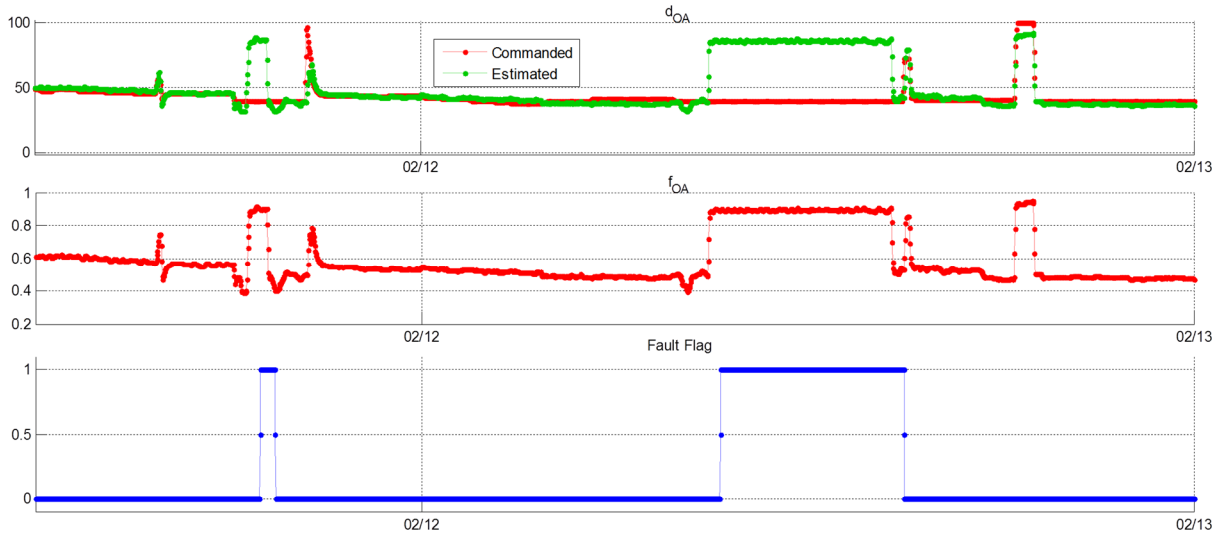

Figure 5. Illustration of validation test data for the FDD algorithm associated with outdoor air damper Outdoor air damper: BAS command, which was overridden; estimated position (top); outdoor air fraction (middle); fault flag (bottom)

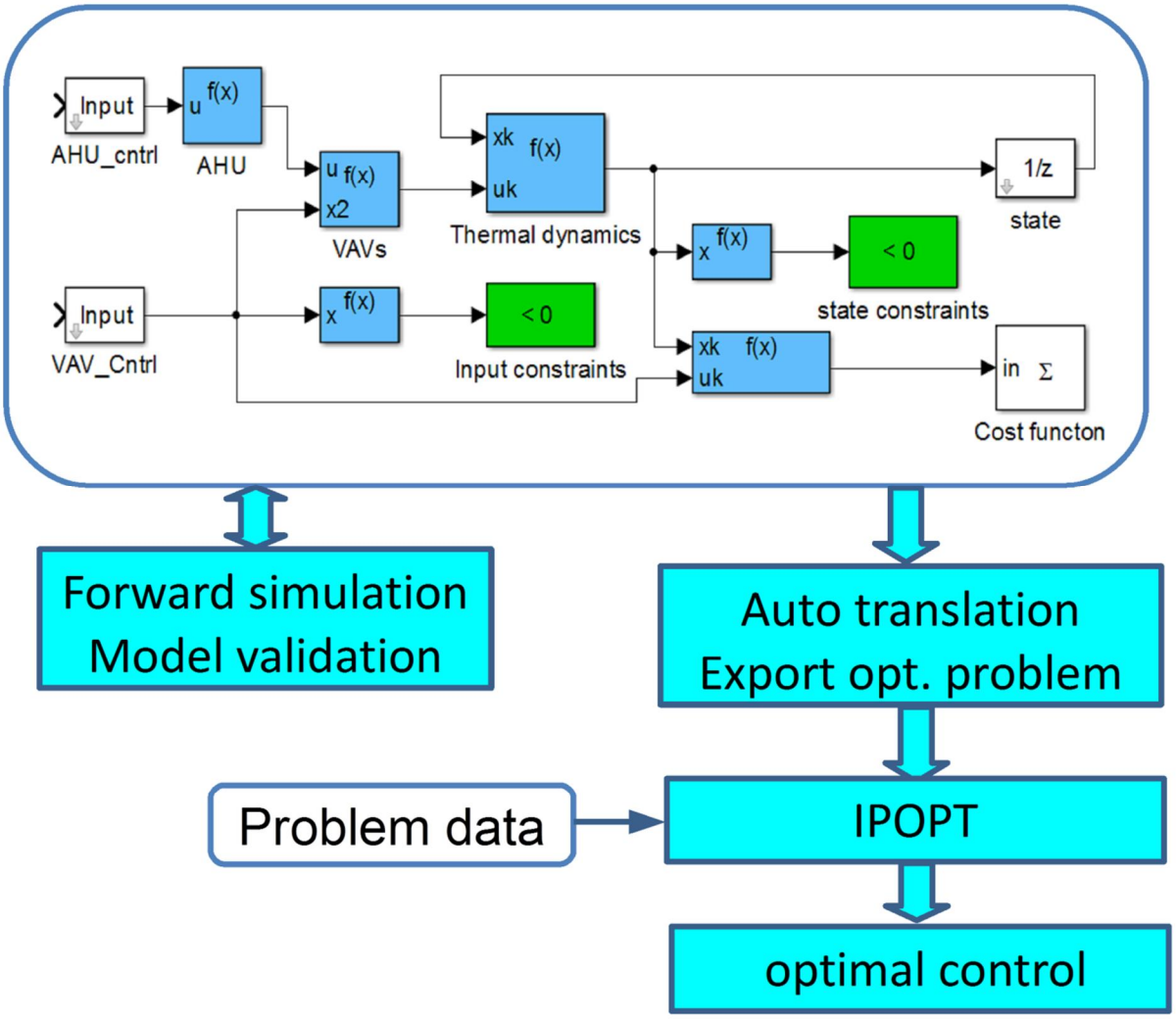

Figure 6. The main steps for converting the MPC algorithm into an optimization problem formulation using BLOM

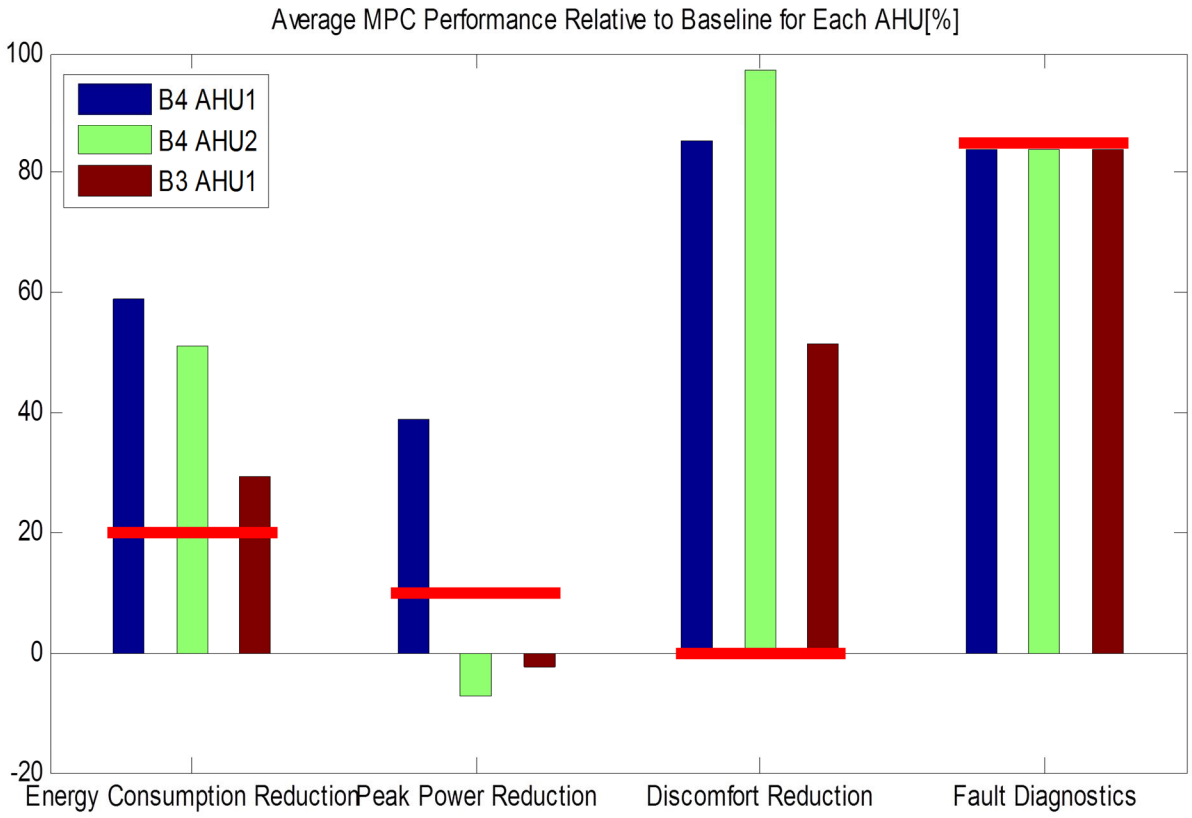

Figure 7. Illustration of the overall results generated during the demonstrations for MPC and FDD algorithms for each of the AHUs for the following objectives: energy consumption reduction, peak power reduction, thermal discomfort reduction, and fault diagnostics system robustness

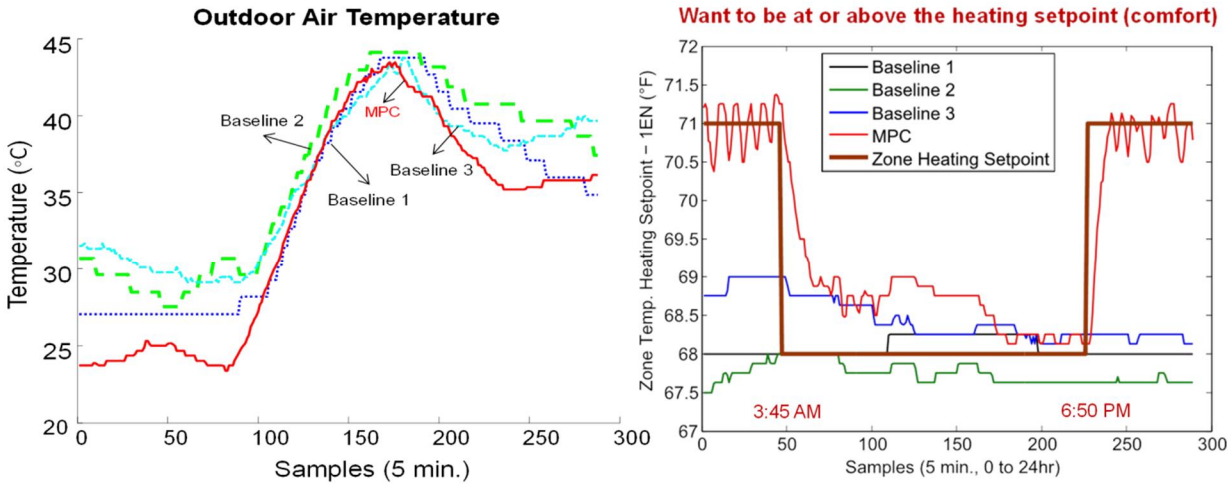

Figure 8. Illustration of ambient temperature during an MPC demonstration day (red) and selected baseline days with similar ambient temperature pattern (left). Temperature values corresponding the MPC and baseline controllers for the same days (right).

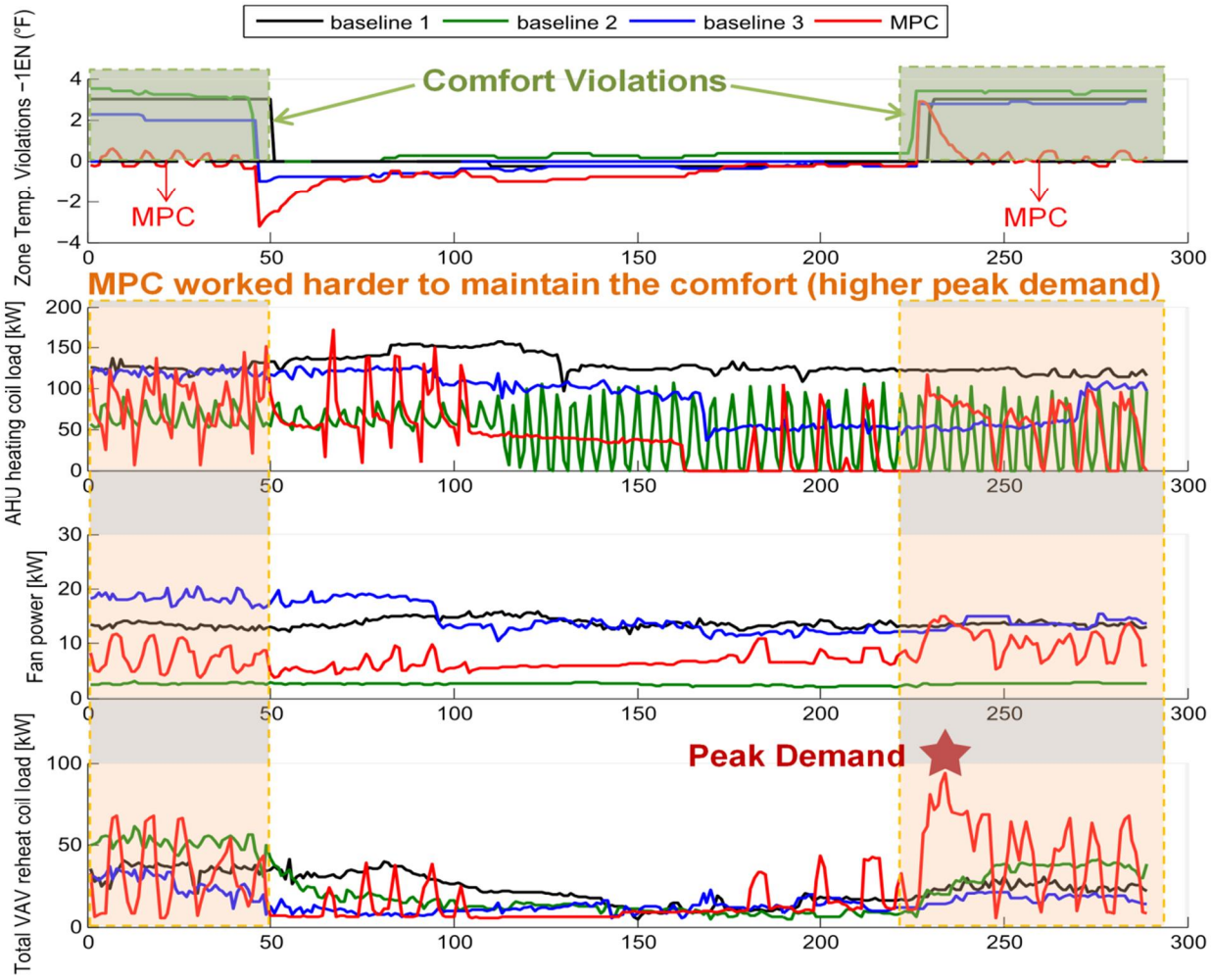

Figure 9. Illustration of temperature comfort violations, AHU heating coil power, fan power and total VAV thermal power during the same days as those illustrated in Figure 8.

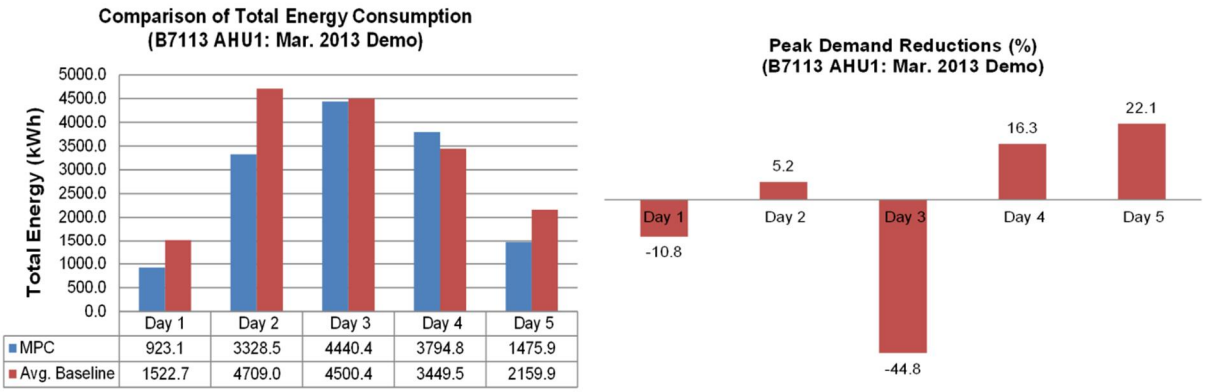

Figure 10. Total energy consumption (left) and peak power reductions (right) of MPC and baseline algorithms. This is a part of the Set I data mentioned in Table 5.

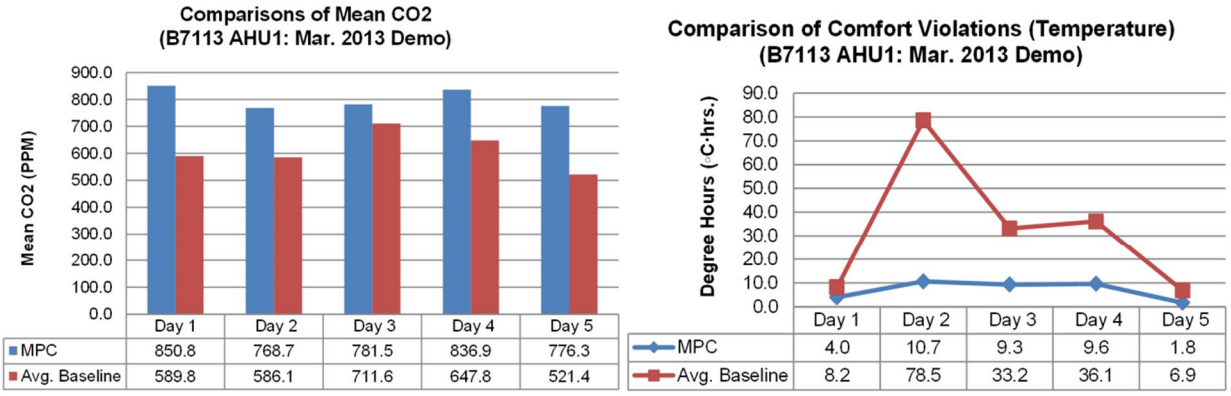

Figure 11. Mean zone CO_2 levels (left) and temperature comfort violation levels (right) for MPC and baseline algorithms. This is a part of the Set I data mentioned in Table 5.

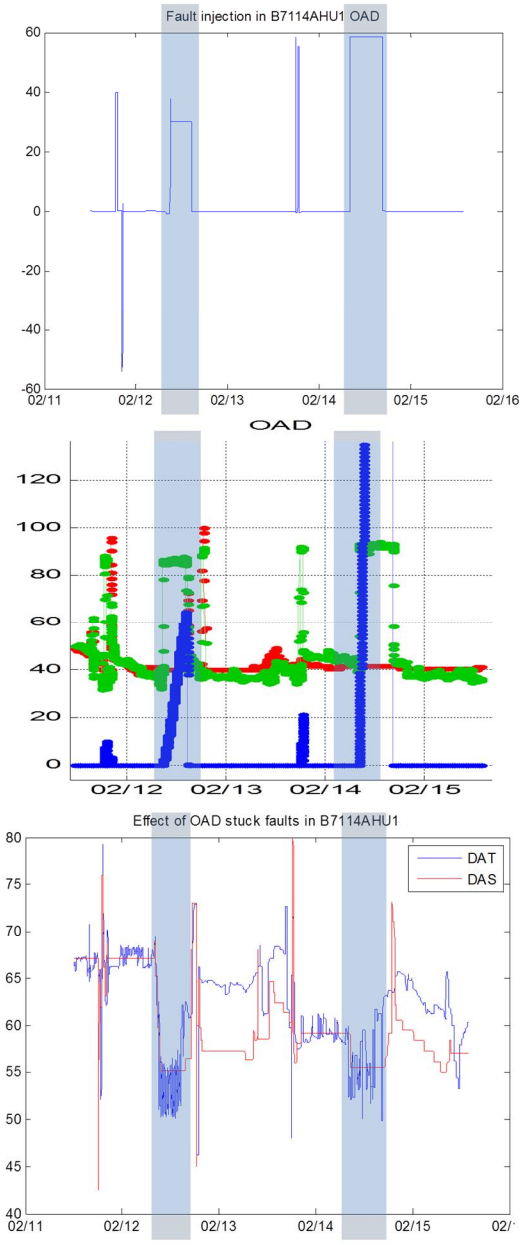

Figure 12. Execution of the fault-seeding and fault-accommodation sequence: OAD faults are executed by overriding the BASôs command (top); the faults are detected by the FDD algorithm (middle); and the FTC algorithms updates the OAD constraints (bottom). The highlighted time intervals correspond to the fault-seeding intervals.

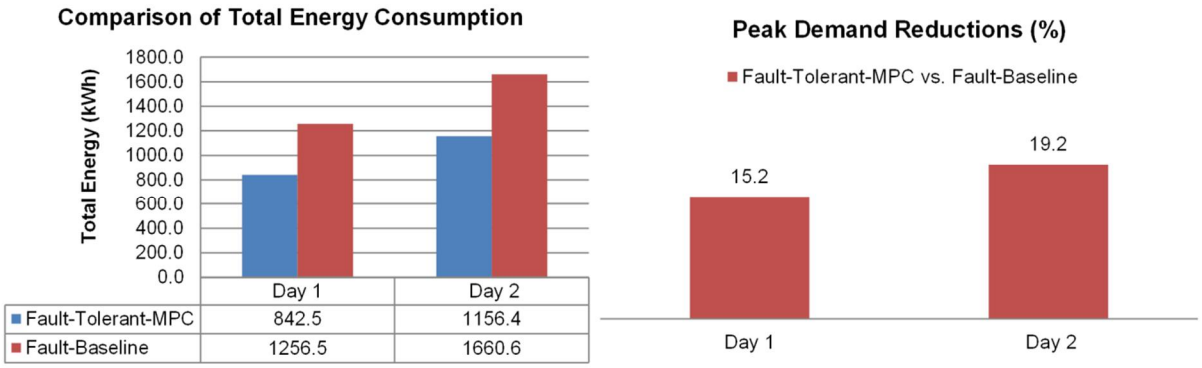

Figure 13. Total energy consumption (left) and peak power reductions (right) of BMSôs control logic and FTC algorithms. This is a part of the Set III data mentioned in Table 5.

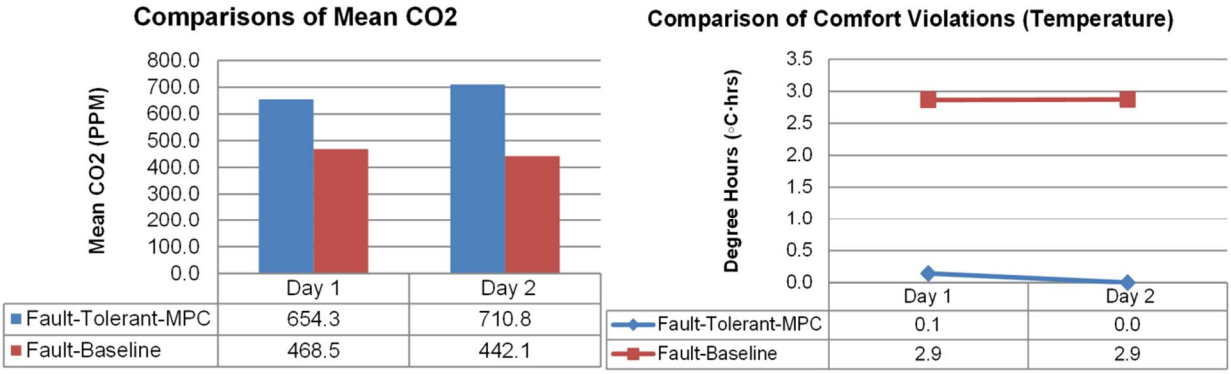

Figure 14. Mean zone CO_2 levels (left) and temperature comfort violation levels (right) for BMSôs control logic and FTC algorithm. This is a part of the Set III data mentioned in Table 5.

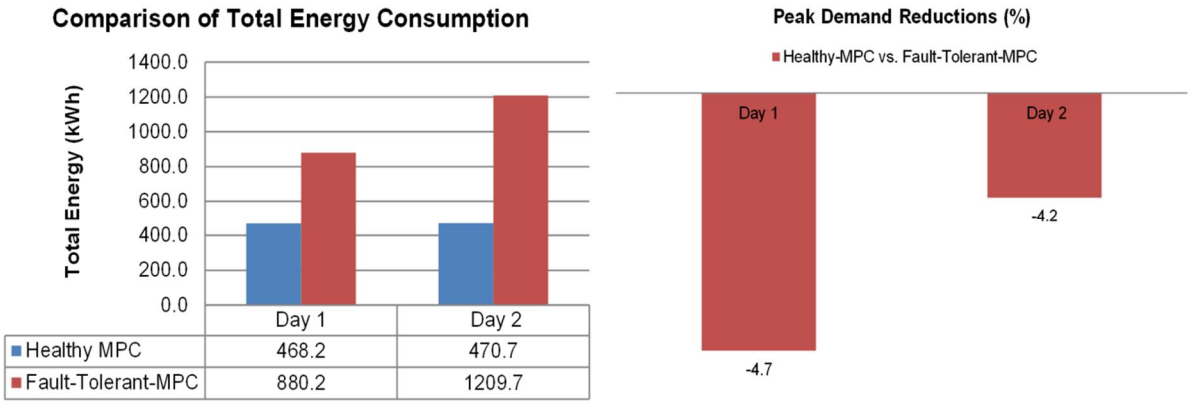

Figure 15. Total energy consumption (left) and peak power reductions (right) of MPC and FTC algorithms. This is a part of the Set IV data mentioned in Table 5.

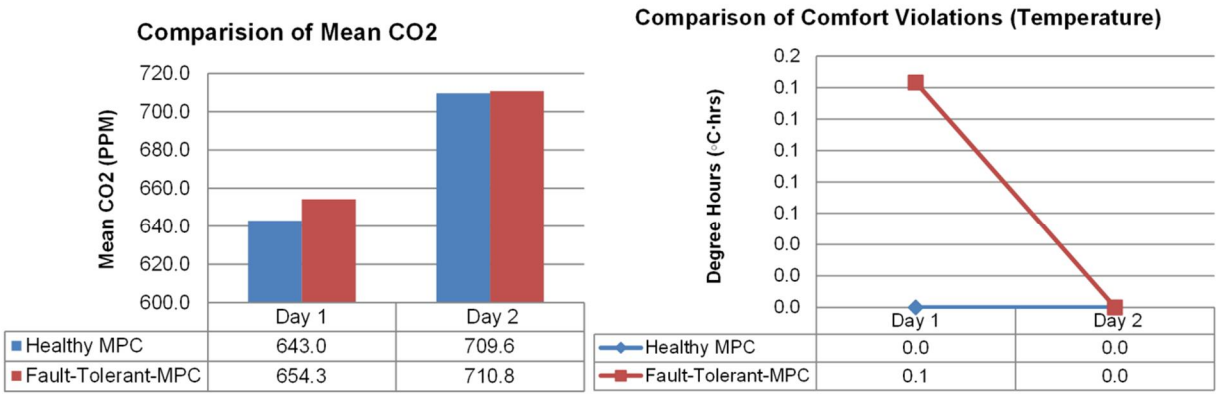

Figure 16. Mean zone CO_2 levels (left) and temperature comfort violation levels (right) for MPC and FTC algorithms. This is a part of the Set IV data mentioned in Table 5.

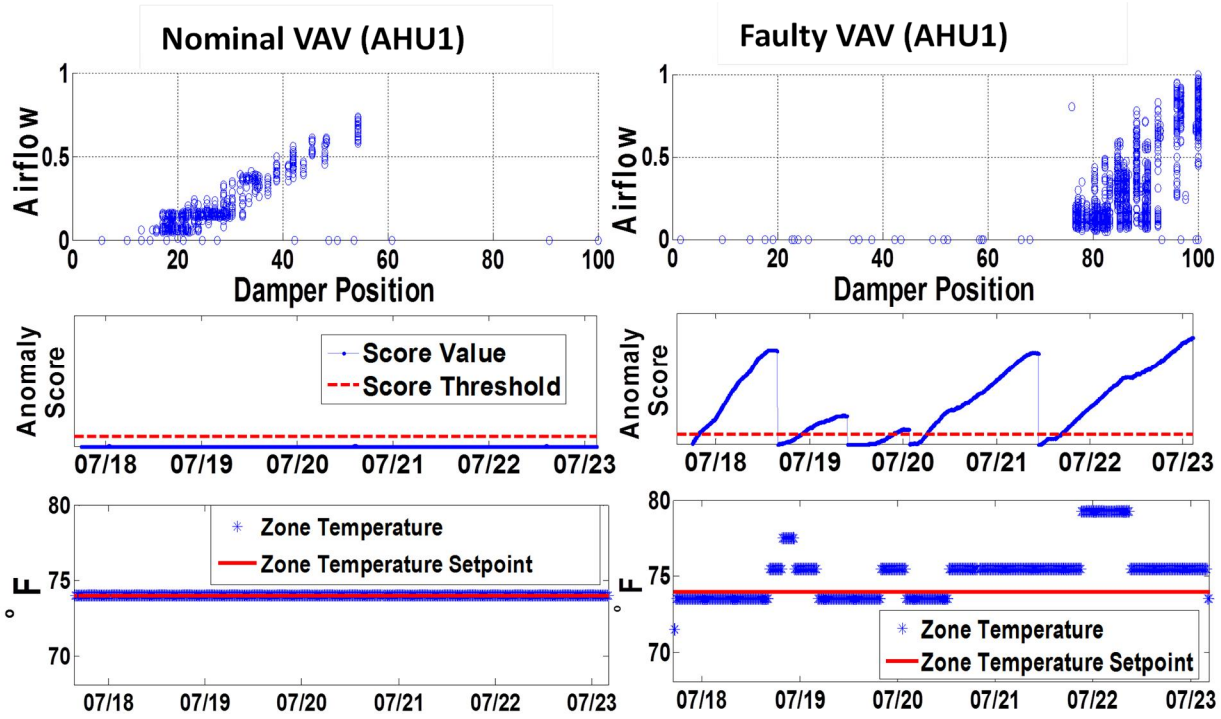

Figure 17. Comparisons between nominal (healthy) and faulty VAV units

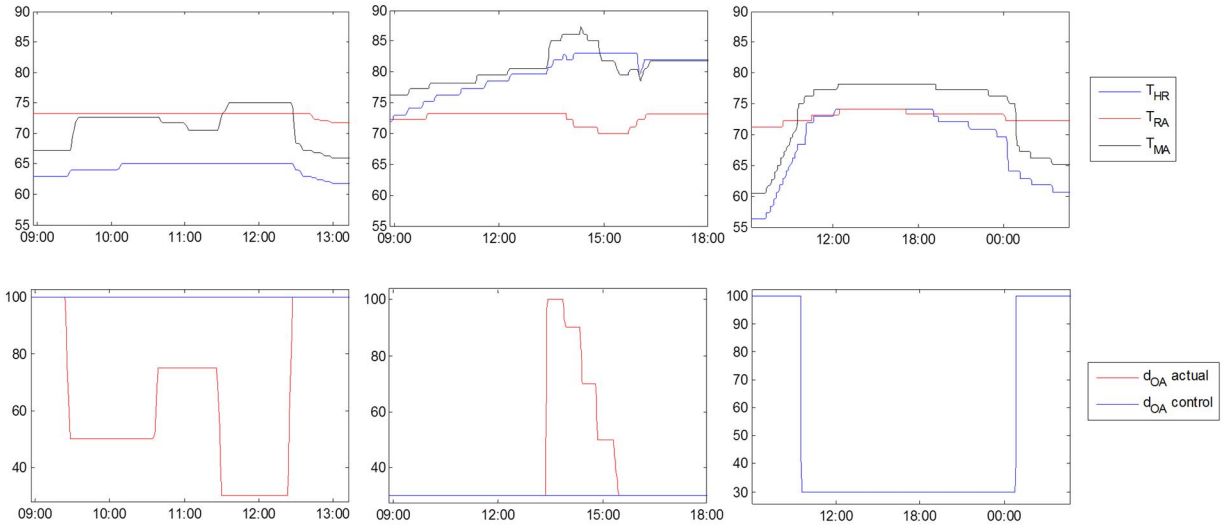

Figure 18. Illustration of the outdoor air damper positions and impacted temperatures for three scenarios described in Figure 12.